EPJ Web of Conferences **274**, 07003 (2022) https://doi.org/10.1051/epjconf/202227407003
XVth Quark Confinement and the Hadron Spectrum

Phases and condensates in zero-temperature QCD at finite μ_I and μ_S

Jens O. Andersen[1,*]

[1]Department of Physics, Faculty of Natural Sciences, Norwegian University of Science and Technology, Høgskoleringen 5, Trondheim, N-7491, Norway,
Niels Bohr International Academy, Blegdamsvej 17, DK-2100 Copenhagen, Denmark

Abstract. I discuss pion and kaon condensation and the the properties of the phases of QCD at finite isospin chemical potential μ_I and strangeness chemical potential μ_S at zero temperature using three-flavor chiral perturbation theory. Electromagnetic effects are included in the calculation of the phase diagram, which implies that the charged meson condensed phases become superconducting phases of QCD with a massive photon via the Higgs mechanism. Without electromagnetic effects, we show results for the light quark condensate and the pion condensate as functions of μ_I at next-to-leading (NLO) order in the low-energy expansion. The results are compared with recent lattice simulations and by including the NLO corrections, one obtains very good agreement.

1 Introduction

In this talk, I would like to discuss various aspects of the phases of QCD at zero temperature, but finite isospin and strangeness density. However, before I do that, I will briefly comment on the QCD phase diagram as it is normally presented, namely in the μ_B–T plane. It is shown in Fig. 1, borrowed from Ref. [1]. Few of the results for the phase diagram are rigorous in the sense that they are obtained from first principles, rather they are obtained by model calculations. However, for asymptotically high temperatures and zero baryon chemical potential, we know that QCD is in a quark-gluon plasma phase consisting of weakly interacting deconfined quarks and gluons. Similarly, we know that at asymptotically high baryon density and zero temperature, QCD is in the color-flavor locked phase arising from an attracting channel of one-gluon exchange and the resulting instability of the Fermi surface. From lattice simulations, we know that there is a cross-over transition for $\mu_B = 0$ at a temperature of around 155 MeV. For low temperatures and large chemical potentials, the infamous sign problem, prohibits the use of standard Monte Carlo techniques to study the properties of QCD. One must therefore resort to low-energy models such as the NJL model and the quark-meson model. Over the past two decades, a huge amount of work has been done to map out the phase diagram.

The situation is even more complex than this since, instead of using a common quark chemical potential for all quarks, one can introduce a separate chemical potential μ_f for each

*e-mail: andersen@tf.phys.ntnu.no

flavor. For three flavors, we use either μ_u, μ_d, and μ_s or the baryon chemical potential μ_B, the isospin chemical potential μ_I, and strangeness chemical potential μ_S defined as

$$\mu_B = \frac{3}{2}(\mu_u + \mu_d) , \qquad \mu_I = \mu_u - \mu_d , \qquad \mu_S = \frac{1}{2}(\mu_u + \mu_d - 2\mu_s) . \tag{1}$$

For $\mu_B = \mu_S = 0$ but nonzero μ_I, one can carry out Monte Carlo simulations using standard techniques since the fermion determinant in this case is real and consequently there is no sign problem. This opens up the possibility to study charged pion condensation on the lattice and confront it with results from low-energy effective theories. In this talk, I will discuss pion condensation for two and three flavors using chiral perturbation theory (χPT) as a low-energy effective theory for QCD and show results for the light quark and pion condensates as a function of μ_I with $\mu_B = \mu_S = 0$. The results will be compared to recent high-precision lattice simulations [2–5]. I will also discuss the phase diagram and meson condensation for three flavors in the μ_I–μ_S plane at zero temperature, with and without electromagnetic interactions.

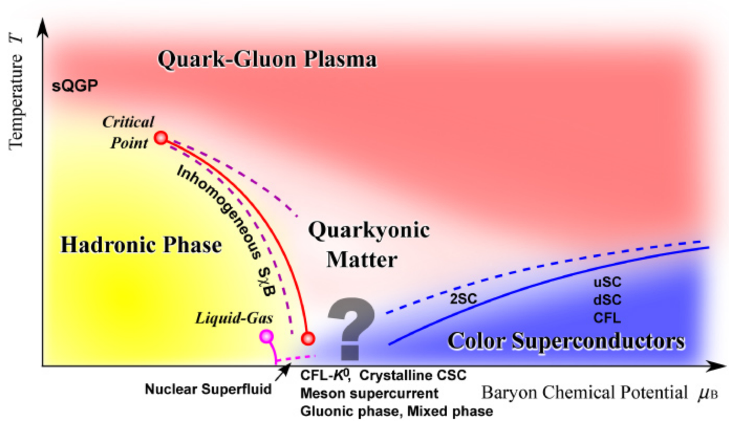

Figure 1. Phase diagram of QCD in the μ_B–T plane. Figure from Ref. [1].

In Fig. 2, we sketch the phase diagram of two-flavor QCD in the the μ_I–T plane. In the lower left region, we have the hadronic phase where chiral symmetry is broken and quarks are confined. As the temperature increases, one enters the quark-gluon plasma phase. Along the μ_I-axis, there is a transition from the hadronic phase to a Bose-condensed phase of charged pions. In this phase, the $U(1)_{I_3}$ symmetry is broken giving rise to a massless Goldstone boson, which is a mixture of π^+ and π^-. For large isospin chemical and low temperature, one expects that quarks are the relevant degrees of freedom rather than pions [6] . The Fermi surface that exists when the interactions are turned off, is rendered unstable once they are turned on, since they are attractive. The system is then described in terms of loosely bound Cooper pairs instead of tightly bound pions. Since the symmetry breaking pattern is the same, there is a cross-over transition rather than a true phase transition between the BEC and the BCS phases [6].

2 χPT at finite isospin chemical potential μ_I

We will be using chiral perturbation theory to describe the pion-condensed phase of QCD at finite μ_I and zero temperature. χPT is a low-energy effective theory for QCD based on

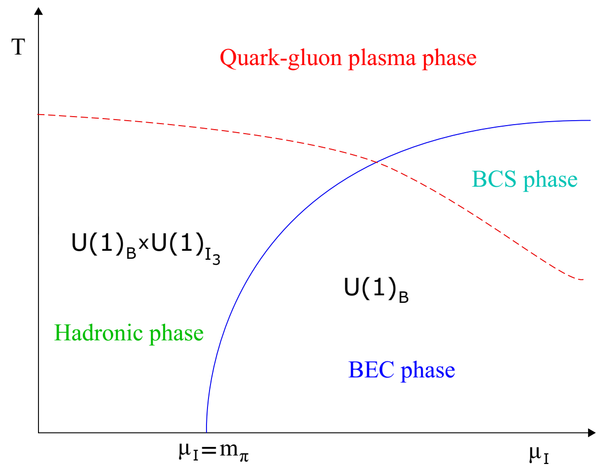

Figure 2. Phase diagram of QCD in the μ_I–T plane.

the (global) symmetries and degrees of freedom. It provides a correct model-independent description as long as one is inside its domain of validity [7–9]. The effective Lagrangian that describes the low-energy degrees of freedom of QCD (pions, kaons, eta) can be written in a low-energy expansion,

$$\mathcal{L} \;=\; \mathcal{L}_2 + \mathcal{L}_4 + \ldots\,, \tag{2}$$

where the subscript denotes the order in the expansion. The expansion parameter can be written as $\frac{M}{4\pi f}$ with M being a relevant mass or momentum scale and f is the pion-decay constant. The leading-order Lagrangian is the nonlinear sigma model, which for two flavors reads

$$\mathcal{L}_2 \;=\; \frac{1}{4}f^2\langle\nabla_\mu\Sigma\nabla^\mu\Sigma^\dagger\rangle + \frac{1}{4}f^2\langle\chi^\dagger\Sigma + \Sigma^\dagger\chi\rangle\,, \tag{3}$$

where $\langle\rangle$ means trace in flavor space and

$$\Sigma = e^{i\frac{\phi_a\tau_a}{f}}\,, \qquad\qquad \chi = 2B_0\mathrm{diag}(m_u, m_d)\,, \tag{4}$$

with ϕ_a being the Goldstone bosons fields, $m_{u,d}$ are the quark masses, and B_0 is the related to the tree level quark condensate in the vacuum via $\langle\bar{\psi}\psi\rangle = -f^2B_0$. The covariant derivative is

$$\nabla_\mu\Sigma \equiv \partial_\mu\Sigma - i\left[v_\mu, \Sigma\right]\,, \tag{5}$$

with $v_\mu = \delta_{\mu0}(\frac{1}{3}\mu_B\mathbb{1} + \frac{1}{2}\mu_I\tau_3)$. Note that our results will be independent of μ_B since the unit matrix $\mathbb{1}$ commutes with everything, this reflects that the mesons have zero baryon number.

The most general ansatz for the normalized ground state can after some simplifications be written as [6]

$$\Sigma_\alpha \;=\; \mathbb{1}\cos\alpha + i\tau_2\sin\alpha = e^{i\alpha\tau_2} = \begin{pmatrix} \cos\alpha & \sin\alpha \\ -\sin\alpha & \cos\alpha \end{pmatrix}\,, \tag{6}$$

which simply is a rotation in flavor space of the vacuum state $\mathbb{1}$ by an angle α. The leading-order thermodynamic potential is

$$\Omega_0 \;=\; -f^2B_0(m_u + m_d)\cos\alpha - \frac{1}{2}f^2\mu_I^2\sin^2\alpha\,. \tag{7}$$

We see that there is a competition between the two terms in Eq. (7), the first term prefers the vacuum state $\alpha = 0$, while the second term prefers $\alpha = \frac{1}{2}\pi$. The optimum is found by balancing these two terms in the thermodynamic potential,

$$\cos\alpha = \frac{m_{\pi,0}^2}{\mu_I^2}\,, \qquad \mu_I^2 \geq m_{\pi,0}^2\,, \tag{8}$$

$$\alpha = 0\,, \qquad \mu_I^2 < m_{\pi,0}^2\,, \tag{9}$$

where $m_{\pi,0}^2 = B_0(m_u + m_d)$ is the tree-level pion mass. Thus there is a phase transition from the vacuum to a pion-condensed phase at a critical μ_I, $\mu_I^c = \pm m_{\pi,0}$. To determine the order of the transition, one can construct a Ginzburg-Landau energy functional by expanding the thermodynamic potential Ω_0 around $\alpha = 0$,

$$\Omega_0 = -f^2 m_{\pi,0}^2 + \frac{1}{2}f^2[m_{\pi,0}^2 - \mu_I^2]\alpha^2 - \frac{1}{24}f^2\left[m_{\pi,0}^2 - 4\mu_I^2\right]\alpha^4 + O(\alpha^6)\,. \tag{10}$$

We define a critical chemical isospin potential μ_I^c when the order-α^2 term vanishes, i.e. $\mu_I^c = \pm m_{\pi,0}$. Since the coefficient of the order-α^4 term is positive for $\mu_I = \mu_I^c$, the transition is second order. Note that all thermodynamic quantities are independent of μ_I for $\mu_I^2 < m_{\pi,0}^2$ implying that e.g. the isospin density vanishes in the same region and not only for $\mu_I = 0$. This is an example of the Silver-Blaze property [10].

3 Phase diagram for three flavors

We next consider the phase diagram for three-flavor QCD at finite μ_I and μ_S including electromagnetic effects. If we couple χPT to dynamical photons, the Lagrangian contains a few extra terms at leading order in the low-energy expansion [11],

$$\begin{aligned}\mathcal{L}_2 &= -\frac{1}{4}F_{\mu\nu}F^{\mu\nu} + \frac{1}{4}f^2\langle\nabla_\mu\Sigma\nabla^\mu\Sigma^\dagger\rangle + \frac{1}{4}f^2\langle\chi^\dagger\Sigma + \Sigma^\dagger\chi\rangle + C\langle Q\Sigma Q\Sigma^\dagger\rangle \\ &\quad + \mathcal{L}_{\rm gf} + \mathcal{L}_{\rm ghost}\,,\end{aligned} \tag{11}$$

with $\chi = 2B_0\mathrm{diag}(m_u, m_d, m_s)$ and $\Sigma = e^{i\frac{\phi_a\lambda_a}{f}}$. The new term $C\langle Q\Sigma Q\Sigma^\dagger\rangle$ is responsible for the tree-level mass splitting of the charged and neutral pions, and it also contributes to the tree-level mass splitting between the charged and neutral kaons. The inclusion of electromagnetic effects also implies that the phases with charged meson condensates are superconducting and that the massless degree of freedom (the Goldstone boson) is eaten up by the photon which becomes massive via the Higgs mechanism. The term v_μ in the covariant derivative Eq. (5) is replaced by

$$v_0 = \tfrac{1}{3}(\mu_B - \mu_S)\mathbb{1} + \tfrac{1}{2}\mu_{K^\pm}\lambda_Q + \frac{1}{2}\mu_{K^0}\lambda_K\,, \qquad v_i = 0\,, \tag{12}$$

where

$$\mu_{K^\pm} = \frac{1}{2}\mu_I + \mu_S\,, \qquad \mu_{K^0} = -\frac{1}{2}\mu_I + \mu_S\,, \tag{13}$$

$$\lambda_Q = \lambda_3 + \frac{1}{\sqrt{3}}\lambda_8\,, \qquad \lambda_K = -\lambda_3 + \frac{1}{\sqrt{3}}\lambda_8\,. \tag{14}$$

In analogy with the two-flavor case, we expect onset of charged kaon condensation when $\mu_{K^\pm}^2 = m_{K^\pm}^2$ and neutral kaon condensation when $\mu_{K^0}^2 = m_{K^0}^2$. The corresponding ansätze for the ground states are [1]

$$\Sigma_\beta = e^{i\beta\lambda_5} = \begin{pmatrix} \cos\beta & 0 & \sin\beta \\ 0 & 1 & 0 \\ -\sin\beta & 0 & \cos\beta \end{pmatrix}, \quad \Sigma_\gamma = e^{i\gamma\lambda_7} = \begin{pmatrix} 1 & 0 & 0 \\ 0 & \cos\gamma & \sin\gamma \\ 0 & -\sin\gamma & \cos\gamma \end{pmatrix}. \tag{15}$$

The thermodynamic potential in the different phases can then be computed as functions of the chemical potentials. For example, in the charged kaon condensed phase, the thermodynamic potential is

$$\Omega_0 = -f^2 B_0(m_u + m_s)\cos\alpha - \frac{1}{2}f^2\left[\mu_{K^\pm}^2 - \Delta m_{\mathrm{EM}}^2\right]\sin^2\alpha\ , \tag{16}$$

where $\Delta m_{\mathrm{EM}}^2 = \frac{2Ce^2}{f^2}$ is the splitting between the charged and neutral kaons due to electromagnetism. It follows that the transition takes place exactly at $\mu_{K^\pm}^2 = m_{K^\pm}^2 = B_0(m_u + m_d) + \frac{2Ce^2}{f^2}$ as expected.

For each value of (μ_I, μ_S), we find the phase with the lowest value of Ω_0 (or largest pressure). This phase wins and we can map out the phase diagram in this manner. The result is shown in the left panel of Fig. 3. The black lines are the transition lines without electromagnetic interactions and the red lines are with electromagnetic interactions. The former was first obtained by Kogut and Toublan [12] in the isospin limit. The phases with charged meson condensation become Higgs phases upon including electromagnetic effects, with a tree-level mass of the photon of $m_A = ef\sin\alpha$. The transitions from the normal phase to a meson-condensed phase is always second order with mean-field exponents in the $O(2)$ universality class. The transitions between the various condensed phases are always first order and involve the competition between the order parameters of the different phases. As we cross the transition lines, the order parameters as well as the isospin and strangeness densities, n_I and n_S jump discontinuously. The small offset of the dashed vertical lines is due to the mass difference between the charged and neutral kaons, which is both due to $\Delta m_{\mathrm{EM}} \neq 0$, and $m_u \neq m_d$. These contributions, however, pull in opposite directions, as we see in the phase diagram. The contribution due to the difference in quark masses adds to the mass of the $K^0/\bar{K}^0$ meson, which is why the black transition line between the kaon condensate is to the left of the $\mu_I = 0$ line, while the electromagnetic contribution adds to the mass of the charged kaon, which is why the red line is between these two lines. The partition function in the normal phase is independent of the two chemical potentials μ_I and μ_S, which again is the Silver Blaze property [10]. In the right panels, we have zoomed in on the triple points. Upper panel shows the intersection of the normal, neutral kaon condensed and charged kaon condensed phases, while the lower shows the intersection of the normal, pion condensed, and charged kaon condensed phases.

4 $O(p^4)$ calculation of thermodynamic potential

I will next sketch the NLO calculation of the thermodynamic potential. For simplicity I consider two flavors in the isospin limit, $m_u = m_d = m$. The thermodynamic potential can be calculated in a low-energy expansion,

$$\Omega = \Omega_0 + \Omega_1 + ..., \tag{17}$$

[1] One could imagine multiple condensates in parts of the μ_I–μ_S plane, but that is ruled out by actual calculations. The angles β and γ are the rotation angles of the quark condensate into a charged or neutral kaon condensate, respectively.

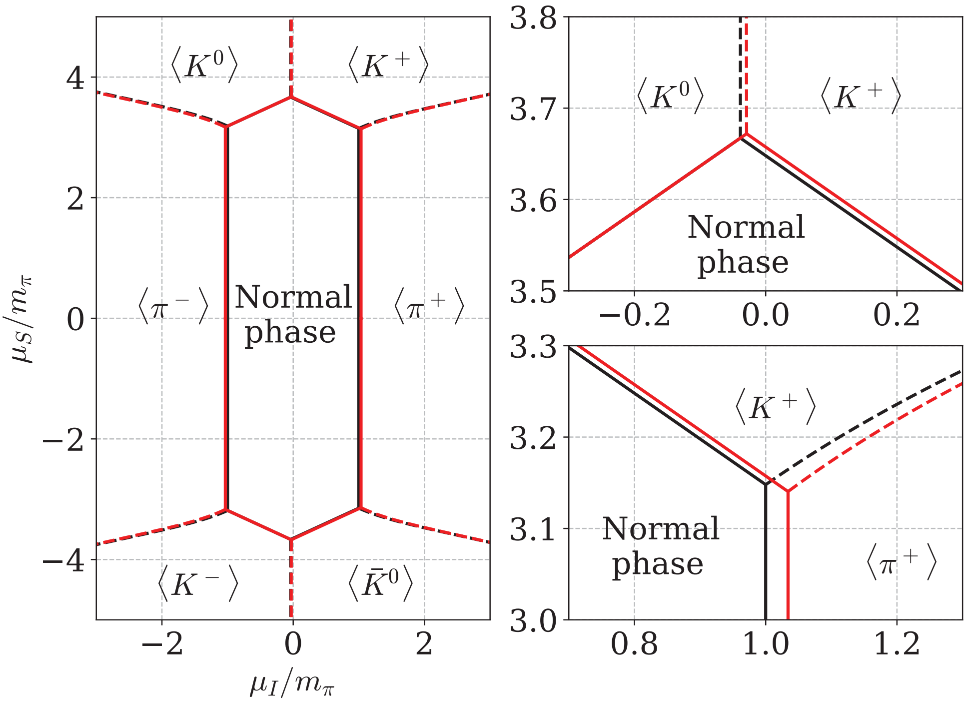

Figure 3. Left panel shows the phase diagram as predicted by χPT in the μ_I–μ_S-plane. In the right panel, we have zoomed in on the triple points. See main text for details. Fig. from Ref. [13].

where Ω_n is the order-$\mathcal{O}(p^{2n+2})$ contribution. The term Ω_1 receives contributions from the one-loop graphs of $\mathcal{L}_2^{\rm quadratic}$ and counterterms coming from $\mathcal{L}_4^{\rm static}$. The relevant terms are

$$\begin{aligned}
\mathcal{L}_2^{\rm quadratic} &= \tfrac{1}{2}(\partial_\mu\phi_a)(\partial^\mu\phi_a) + \mu_I\cos\alpha(\phi_1\partial_0\phi_2 - \phi_2\partial_0\phi_1) \\
&\quad -\tfrac{1}{2}\Big[(m_{\pi,0}^2\cos\alpha - \mu_I^2\cos^2\alpha)\phi_1^2 + (m_{\pi,0}^2\cos\alpha - \mu_I^2\cos 2\alpha)\phi_2^2 \\
&\quad +(m_{\pi,0}^2\cos\alpha + \mu_I^2\sin^2\alpha)\phi_3^2\Big]\ , \qquad (18) \\
\mathcal{L}_4^{\rm static} &= (l_1+l_2)\mu_I^4\sin^4\alpha + l_4 m_{\pi,0}^2\mu_I^2\cos\alpha\sin^2\alpha + (l_3+l_4)m_{\pi,0}^4\cos^2\alpha + h_1 m_{\pi,0}^4\ , \\
&\quad , \qquad (19)
\end{aligned}$$

where l_1–l_4 and h_1 are bare couplings. They are related to the renormalized couplings l_i^r and h_i^r via $l_i = l_i^r(\Lambda) + \frac{\gamma_i\Lambda^{-2\epsilon}}{2(4\pi)^2}\left[\frac{1}{\epsilon}+1\right]$ and $h_i = h_i^r(\Lambda) + \frac{\delta_i\Lambda^{-2\epsilon}}{2(4\pi)^2}\left[\frac{1}{\epsilon}+1\right]$, where γ_i, δ_i are coefficients and Λ is the renormalization scale in the $\overline{\rm MS}$ scheme. Since $\delta_1 = 0$, $h_1 = h_1^r$ and does not run. Performing the Gaussian integral over the quantum fields ϕ_a in dimensionsal regularization using Eq. (18), we obtain a divergent contribution to Ω_1. The divergences are cancelled by adding the quartic terms from Eq. (19) and renormalizing the couplings by replacing the bare couplings with the renormalized ones. The final result is

$$\begin{aligned}\Omega_0+\Omega_1 &= -f^2 m_{\pi,0}^2\cos\alpha-\frac{1}{2}f^2\mu_I^2\sin^2\alpha\\ &\quad-\frac{1}{4(4\pi)^2}\left[\frac{3}{2}-\bar{l}_3+4\bar{l}_4+\log\left(\frac{m_{\pi,0}^2}{\tilde{m}_2^2}\right)+2\log\left(\frac{m_{\pi,0}^2}{m_3^2}\right)\right]m_{\pi,0}^4\cos^2\alpha\\ &\quad-\frac{1}{(4\pi)^2}\left[\frac{1}{2}+\bar{l}_4+\log\left(\frac{m_{\pi,0}^2}{m_3^2}\right)\right]m_{\pi,0}^2\mu_I^2\cos\alpha\sin^2\alpha\\ &\quad-\frac{1}{4(4\pi)^2}\left[1+\frac{2}{3}\bar{l}_1+\frac{4}{3}\bar{l}_2+2\log\left(\frac{m_{\pi,0}^2}{m_3^2}\right)\right]\mu_I^4\sin^4\alpha\\ &\quad-\frac{1}{(4\pi)^2}\bar{h}_1 m_{\pi,0}^4+V_{1,\pi^+}^{\rm fin}+V_{1,\pi^-}^{\rm fin}\,, \end{aligned}\tag{20}$$

where $\tilde{m}_2^2 = m_{\pi,0}^2\cos\alpha$, $m_3^2 = m_{\pi,0}^2+\mu_I^2\sin^2\alpha$, and $V_{1,\pi^+}^{\rm fin}+V_{1,\pi^-}^{\rm fin}$ are two complicated finite terms that must be evaluated numerically. Finally, $\bar{l}_i$ and $\bar{h}_i$ are, up to a prefactor, equal to l_i^r and h_i^r at the scale $\Lambda = m_{\pi,0}$. Using Eq. (20) one can show that the phase transition takes place at $\mu_I^c = m_\pi$, where the physical pion mass m_π now includes radiative corrections [8], see Eq. (21) below. The parameters $\bar{l}_i$ are determined by experiment and $\bar{h}_1$ estimated by model calculations. The parameters $m_{\pi,0}^2 = 2B_0 m$ and f can be found by inverting the one-loop relations using the experimental values for the pion mass and the pion decay constant,

$$m_\pi^2 = m_{\pi,0}^2\left[1-\frac{m_{\pi,0}^2}{2(4\pi)^2f^2}\bar{l}_3\right]\,,\qquad f_\pi^2 = f^2\left[1+\frac{2m_{\pi,0}^2}{(4\pi)^2f^2}\bar{l}_4\right]\,. \tag{21}$$

5 Condensates

In order to obtain the light quark and pion condensates, we need to calculate the thermodynamic potential Ω with sources m and j, where the latter is a pionic source. The former has already been included in the calculations I have shown and it is also straightforward to include a pionic source j in the calculations. For example, in the two-flavor expression for the thermodynamic potential, one simply makes the replacements $m\cos\alpha \to m\cos\alpha + j\sin\alpha$ and $\bar{h}_1 m_{\pi,0}^4 = \bar{h}_1(2B_0m)^2 \to \bar{h}_1[(2B_0m)^2+(2B_0j)^2]$ [14]. Once these replacements are made, the condensates are given by

$$\langle\bar{\psi}\psi\rangle_{\mu_I} = \frac{1}{2}\frac{\partial\Omega}{\partial m} = -f^2B_0\cos\alpha+\ldots\,,\qquad \langle\pi^+\rangle_{\mu_I} = \frac{1}{2}\frac{\partial\Omega}{\partial j} = -f^2B_0\sin\alpha+\ldots\,, \tag{22}$$

where I on the the right-hand side have written explicitly the tree-level contributions. The subscript μ_I on the expectation values indicates that they depend on the isospin chemical potential. Instead of plotting the condensates directly, we define the normalized deviations as

$$\Sigma_{\bar{\psi}\psi} = -\frac{2m}{m_\pi^2f_\pi^2}\left[\langle\bar{\psi}\psi\rangle_{\mu_I}-\langle\bar{\psi}\psi\rangle_0^{j=0}\right]+1\,,\qquad \Sigma_\pi = -\frac{2m}{m_\pi^2f_\pi^2}\langle\pi^+\rangle_{\mu_I}\,. \tag{23}$$

At tree level, Eq. (22) shows the rotation of the quark condensate into a pion condensate. Equivalently, from Eq. (23), the deviations at tree level satisfy $\Sigma_{\bar{\psi}\psi,\rm tree}+\Sigma_{\pi,\rm tree}^2 = 1$. This interpretation no longer holds beyond $O(p^2)$. In the left panel of Fig. 4, we show $\Sigma_{\bar{\psi}\psi}$ as a function of $\frac{\mu_I}{m_\pi}$ at leading order (red line) [2] and next-to-leading order for two flavors (blue line) and

[2]The leading order result is the same for two and three flavors.

three flavor (green line). The data points are from lattice simulations of Ref. [2–5]. In the right panel, we show Σ_π in the same approximations. We note that the difference between $\Sigma_{\bar\psi\psi}$ in the various approximations is very small and they all agree very well with the lattice data points. Regarding Σ_π, we notice that it is nonzero for $\mu_I < m_\pi$, which simply reflects that the curves shown are for nonzero pion source, $j = 0.00517054m_\pi$ The $U(1)_{I_3}$-symmetry is therefore broken explicitly for all values of μ_I. Comparing the various approximations and lattice data, it is evident that including the $O(p^4)$ corrections results in a substantially improved agreement between χPT and simulations. All the numerical results have been obtained by using the same physical meson masses as well as f_π as in the lattice simulations. This requires that we invert the relations Eq. (21) to obtain the values for the bare mass m and the bare pion decay constant f using the experimental values of $\bar{l}_i$.

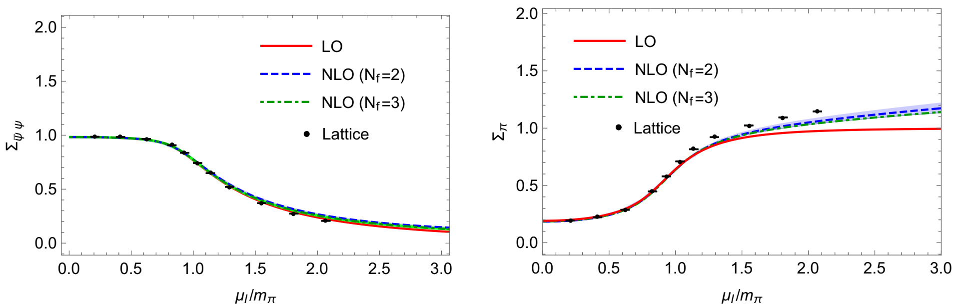

Figure 4. $\Sigma_{\bar\psi\psi}$ (left panel) and Σ_π (right panel) as functions of μ_I/m_π at zero temperature and finite source $j = 0.00517054m_\pi$. Fig. taken from Ref. [14].

6 Acknowledgements

I would like to thank Prabal Adhikari, Martin Mojahed, and Martin Kjøllesdal Johnsrud for collaboration. I would also like to thank the organizers of the XVth Quark confinement and the Hadron spectrum conference for a very interesting meeting.

References

[1] T. Hatsuda, K. Fukushima, Rept. Prog. Phys **74**, 014001 (2011)
[2] B.B. Brandt, G. Endrődi, PoS LATTICE p. 039 (2016)
[3] B.B. Brandt, G. Endrődi, S. Schmalzbauer, EPJ Web Conf. **175**, 07020 (2018)
[4] B.B. Brandt, G. Endrődi, S. Schmalzbauer, Phys. Rev. D **97**, 054514 (2018)
[5] B.B. Brandt, G. Endrődi, Phys. Rev. D **99**, 014518 (2019)
[6] D.T. Son, M. Stephanov, Phys. Rev. Lett **86**, 592 (2001)
[7] S. Weinberg, Physica A **96** (1979)
[8] J. Gasser, H. Leutwyler, Ann. Phys. **158**, 142 (1984)
[9] J. Gasser, H. Leutwyler, Nucl. Phys. **250**, 465 (1985)
[10] T.D. Cohen, Phys. Rev. Lett. **91**, 222001 (2003)
[11] G. Ecker, J. Gasser, A. Pich, E. de Rafael, Phys. Lett. B **321** (1989)
[12] J. Kogut, D. Toublan, Phys. Rev. D **64**, 034007 (2001)
[13] J.O. Andersen, M.K. Johnsrund (2022), `2206.04291`
[14] P. Adhikari, J.O. Andersen, M. Mojahed, Eur. J. Phys. C **81**, 449 (2021)